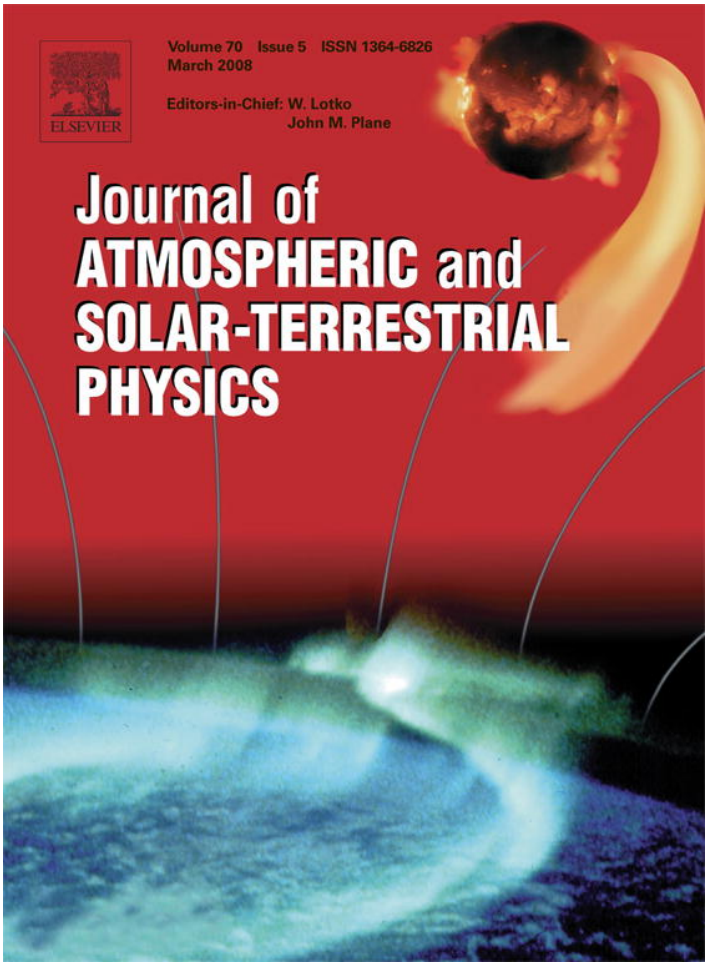

ELSEVIER

Journal of Atmospheric and Solar-Terrestrial Physics 70 (2008) 803–819

Journal of ATMOSPHERIC AND SOLAR-TERRESTRIAL PHYSICS

www.elsevier.com/locate/jastp

The development of new solar indices for use in thermospheric density modeling

W. Kent Tobiska[a,*], S. Dave Bouwer[b,1], Bruce R. Bowman[c,2]

[a]*Space Environment Technologies, Space Weather Division, 1676 Palisades Drive, Pacific Palisades, CA 90272, USA*
[b]*Space Environment Technologies, 986 Croke Drive, Thornton, CO 80260, USA*
[c]*Air Force Space Command, Space Analysis/A9AC, AFSPC/A9AC, Atrium II, Suite 212, 1150 Academy Park Loop, Colorado Springs, CO 80910, USA*

Received 3 July 2007; received in revised form 25 October 2007; accepted 2 November 2007
Available online 17 November 2007

Abstract

New solar indices have been developed to improve thermospheric density modeling for research and operational purposes. Out of 11 new and 4 legacy indices and proxies, we have selected 3 ($F_{10.7}$, $S_{10.7}$, and $M_{10.7}$) for use in the new JB2006 empirical thermospheric density model. In this work, we report on the development of these solar irradiance indices. The rationale for their use, their definitions, and their characteristics, including the IS 21348:2007 spectral category and sub-category, wavelength range, solar source temperature region, solar source feature, altitude region of terrestrial atmosphere absorption at unit optical depth, and terrestrial atmosphere thermal processes in the region of maximum energy absorption, are described. We also summarize for each solar index the facility and instrument(s) used to observe the solar emission, the time frame over which the data exist, the measurement cadence, the data latency, and the research as well as operational availability. The new solar indices are provided in forecast as well as real time and historical time frames (http://SpaceWx.com JB2006 Quicklink). We describe the forecast methodology, compare results with actual data for active and quiet solar conditions, and compare improvements in $F_{10.7}$ forecasting with legacy HASDM and NOAA SWPC forecasts.

Keywords: Thermosphere; Thermosphere models; Neutral density; Solar EUV; IS 21348:2007; Space weather

1. Introduction

1.1. The challenges of space weather

The near-Earth space environment contains abundant energy that affects natural and technological systems. The primary energy sources in the space environment come from dynamical processes related to stellar (including galactic), solar, and planetary (including comets, gas, and dust) evolution. The energy exists in the form of photons,

*Corresponding author. Tel.: +1 310 573 4185; fax: +1 310 454 9665.
E-mail addresses: ktobiska@spacenvironment.net (W.K. Tobiska), dbouwer@spacenvironment.net (S.D. Bouwer), bruce.bowman@peterson.af.mil (B.R. Bowman).
[1]Tel.: +1 303 635 8113.
[2]Tel.: +1 719 556 3710.

1364-6826/$ - see front matter © 2007 Elsevier Ltd. All rights reserved.
doi:10.1016/j.jastp.2007.11.001

particles (neutral and charged), and fields (magnetic, electric, and gravitational) and it is conserved, transferred, or exchanged. In addition to the natural photons, particles, and fields, human activity has added a new component to the near-Earth space environment, i.e., orbital debris. Together, these comprise the domain of the *near-Earth space environment* as shown in Fig. 1.

The short-term variable impact of solar photons, particles, and fields upon the Earth's environment is known as *space weather*. These energy manifestations come primarily from the interaction of solar magnetic phenomena with the solar surface and atmosphere. These phenomena include coronal holes, active regions, plage, and network, as well as flares and coronal mass ejections (CMEs). The result of these interactions is the collective production of energetic photons, electrons, and protons. They make their way to Earth and affect our space-related technology through events such as single-event upsets, latchup, surface charging, electrostatic discharge, high-frequency radio signal loss, polar cap absorption, scintillation, and atmospheric drag upon satellites (NSWP Implementation Plan, 2000).

Accurate and precise orbit determination is complicated by perturbations upon satellite orbits caused by variable neutral atmosphere density and its drag against the spacecraft. Quantifying these density changes in the neutral atmosphere presents a special challenge and has been a topic of active research since the beginning of the space age. Natural density variations are controlled by two energy sources, i.e., primarily by direct solar irradiance photon illumination of and absorption by neutral species as well as secondarily by solar-wind-charged particles that interact with the magnetosphere and ionosphere system to create electric and magnetic fields responsible for subsequently heating the neutral atmosphere. The solar irradiances and solar wind drive the thermosphere–ionosphere–magnetosphere-coupled system with a variety of characteristic forcing and relaxation response times. The response/relaxation times range from minutes to months. Therefore, understanding solar photon and particle forcing of the upper atmosphere is key to predicting the future neutral density state.

Because of the importance of space weather, there are substantive efforts underway to characterize space weather as a coupled, seamless system from the Sun to Earth (NSWP, 2000; CISM Annual Report, 2003). From an operational perspective, this coupling links data streams and models to provide a capability for quantifying recent, current, and future conditions (Tobiska, 2002, 2003, 2005). In particular, advances in near-term operational forecasting have been made and we report on a major milestone accomplishment for mitigating space weather risks, i.e., the development of new solar irradiance indices with improved operational forecasts.

1.2. Rationale for new solar indices and space situational awareness

Space situational awareness (SSA) can be described as the perception (measurement) of space environment elements within a volume of time and space, the comprehension (interpretation) of their meaning, and the projection (prediction) of their status into the near future. There are many space weather challenges to SSA, including making observations, warnings, forecasts, and analyses with the accuracy, precision, resolution, and timeliness

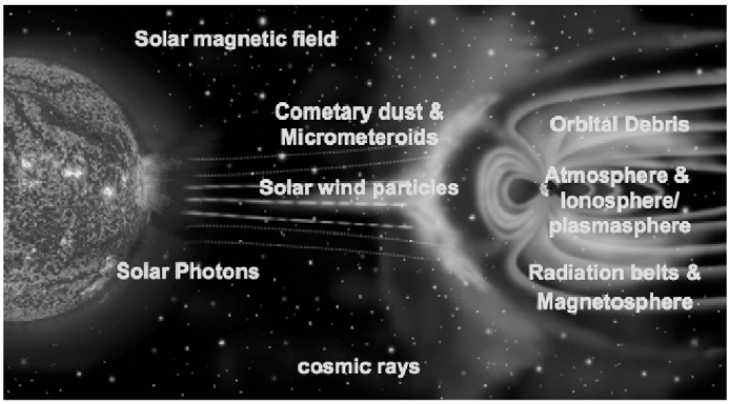

Fig. 1. Space environment components (photons, particles, fields) contribute to space weather (graphic credit NASA).

that are required to meet existing and future requirements. The requirements are derived from classes of missions (communication, navigation, manned space, radar operations, satellite operations, debris monitoring, or surveillance) and there are three requirements' challenges common to all these classes: *making measurements rapidly*, *interpreting them quickly*, *and reacting to real-time and predicted information with appropriate and timely actions*. The capability we have developed will directly support each of these mission classes by meeting these requirements.

For example, solar proxies such as $F_{10.7}$ have only partially fulfilled these common requirements, especially in the context of information interpretation. It has long been realized that components were missing from the solar energy needed for accurate atmospheric density modeling (Tobiska, 1988, 2001; Barth et al., 1990; Viereck et al., 2001; Pardini et al., 2006). This was the motivation for developing additional indices, i.e., to quantify missing solar energy that participates in atmospheric density variations affecting satellite orbits.

The common requirement to make measurements rapidly comes from a need to obtain both high time resolution (usually minutes to hours, depending on the geophysical parameter being measured) and reduced data latency (the time interval between making a measurement and its availability for use). High time resolution generally provides better characterization of physical processes and reduced latency is usually associated with the utility of measurements for decision-making processes. For solar energy related to daily satellite drag and neutral thermosphere variability, daily measurements that are reported within a few hours are rapid enough, with the exception of solar flare events. Our new indices have reduced latency and can be generated with high time resolution.

A requirement to react to real time and predicted information with appropriate and timely actions is a need for expanded data fusion where information content is refined and passed to other processes. Our new indices meet this requirement since they are processed from raw data, modified to represent unique solar energies, and provided to operational users. The result is improved time variability of neutral thermospheric densities at the historical, current, or predicted epochs they are needed.

On-orbit and ground components of space systems serve these mission classes and there are numerous examples of space weather effects upon them. Of immediate relevance are instrument or vehicle anomalies or catastrophic vehicle loss, loss of communications, increased in-space, in-air, on-ground navigation uncertainty, and vehicle or debris orbit change from drag effects. The improved solar irradiance capability we have developed mitigates space weather risks in each of these mission classes.

1.2.1. Communications

High-frequency (HF) signal loss occurs from a change in electron density profiles and thus the reflecting layer of the ionosphere; this can lead to ground-to-ground and ground-to-air communication interruption or loss; it is a transient effect caused in low- and mid-latitudes by soft X-ray ultraviolet (XUV) and extreme ultraviolet (EUV) photons during flares (minutes to hours), as well as by non-photon sources such as solar wind and CME disturbance of the ionosphere through magnetospheric coupling (Goodman, 2005).

1.2.2. Navigation

Total electron content (TEC) variation occurs from a change in the integrated electron density and thus ionosphere column through which GPS signals pass from transmitter to receiver; this can lead to received signal timing error and thus position error in precision navigation systems; it is a transient effect caused in low- and mid-latitudes by XUV–EUV photons during flares (minutes to hours) as well as by non-photon sources such as solar wind and CME disturbance of the ionosphere through magnetospheric coupling (Bishop et al., 2005).

1.2.3. Orbital dynamics

Satellite drag occurs at low Earth orbit (LEO) altitudes from density changes in the neutral thermosphere; this can lead to unmodeled in-track position error that affects satellite operations; it is particularly effective upon satellites without active propulsion and upon orbit debris particles of all sizes including re-entering vehicles; it is a cumulative effect caused in low and mid-latitudes by EUV photons during solar active periods (hours to days) and in high latitudes by Joule heating and particle precipitation (Bowman et al., 2006, 2007).

We note that solar photons interacting with the neutral, then ionized, terrestrial atmosphere are common to these mission classes. The sources for these solar photons at all wavelengths are the solar magnetic-field-induced flare, active region, plage,

network, and internet work (background) radiance features that, summed together, form the full-disk solar irradiance as seen at 1 AU. We have made substantial progress in empirically characterizing how the photons will be effective at or near the Earth and predicting the irradiance fluxes with an accuracy and precision that meets current operational requirements. Our work is part of a coupled data–model system that is improving information content for operational systems in communication, navigation, manned space, radar operations, satellite operations, debris monitoring, and surveillance missions.

1.3. Definitions and IS 21348:2007 compliance

We utilize the new International Standard for determining solar irradiances (IS 21348:2007, 2007). It provides definitions for solar spectral irradiance wavelength ranges and for distinguishing between solar irradiance indices and proxies. The ISO solar spectral irradiance wavelength ranges are used throughout this paper. Solar irradiance indices and proxies, i.e., surrogates for solar irradiances, still have evolving usages of these terms. In general, however, a solar irradiance *proxy* is a measured or modeled data type that is used as a *substitute* for solar spectral irradiances. A solar irradiance *index*, on the other hand, is a measured or modeled data type that is an *indicator* of a solar spectral irradiance activity level. Both can represent line, continua, and integrated irradiances or other irradiance-related solar features such as irradiance deficit from sunspots or sunspot numbers. Solar irradiance proxies and indices have quantifiable values that are related to solar processes and that can be reported through a specified time interval. The new solar indices reported in this work are IS 21348:2007 Type 5 solar irradiance products for the ultraviolet (FUV, EUV, and XUV) and X-ray spectral categories. The processes used for determining solar irradiances reported herein are compliant with *ISO International Standard 21348: Space environment (natural and artificial)—process for determining solar irradiances*.

2. The selection and development of new solar indices for atmospheric heating

We have studied, then developed, a variety of solar indices and proxies to characterize the solar energy absorbed in the atmosphere, which leads to density changes observed by satellites. Table 1 summarizes these solar indices for atmospheric heating, their IS 21348:2007 spectral category, subcategory, wavelength range in units of nm, solar source temperature region, solar source feature, altitude region of terrestrial atmosphere absorption at unit optical depth in units of km, and terrestrial atmosphere thermal region of energy absorption. The indices and proxies marked with an asterisk (*) are those that have been selected for use in the modified Jacchia 1971 atmospheric density model, originally the CIRA72 model (CIRA72, 1972), that is described in a companion paper and is now called the Jacchia–Bowman empirical thermospheric density model (JB2006) (Bowman, et al., 2007). Table 2 summarizes the characteristics of daily solar indices that are highlighted in this study.

In selecting candidate solar indices for driving the thermospheric densities, we first considered the altitudes of unit optical depth for solar photon energy deposition across a variety of wavelengths. This is a derivative of an idea proposed at least three decades ago by Schmidtke (1976), who suggested an EUV proxy summed over wavelength bands. Fig. 2 demonstrates, in a simplified form, the range of unit optical depths we considered by altitude, wavelength, and absorbing species. It became apparent that previous models using $F_{10.7}$ as a solar proxy were primarily considering the heating of atomic oxygen above 180 km by the EUV solar photons. Other wavelengths in the XUV, X-rays, Lyman-α (Lyα), and far ultraviolet (FUV) were not included in empirical modeling formulations. Therefore, our first objective was to correct the missing solar heating by adding a component in the FUV that deposits energy in the lower thermosphere and that is centered on the Schumann–Runge Continuum (SRC) near 155 nm. We additionally considered other mesosphere/lower thermosphere (50–70, 90–125 km) heating processes as well as stratospheric (20–40 km) heating. The results, after removing known effects from the JB2006 model and modeling the residuals with the additional solar emissions, are discussed below as well as in Bowman and Tobiska (2006) and Bowman et al. (2007).

The daily indices we considered in detail, including their source, development, and formulation, were the $F_{10.7}$, $S_{10.7}$, $M_{10.7}$, $XL_{10.7}$, E_{SRC}, and E_{HRT}. The solar proxies or indices all exist through a common time frame, for most indices, of January 1, 1996 through June 12, 2005. Our methodology was to first develop each index or proxy (Tables 1 and 2)

Table 1
Solar indices studied for atmospheric heating

Index	IS 21348 spectral category	IS 21348 spectral sub-category	Wavelength range (nm)	Solar source temperature region[a]	Solar source feature[a]	Atmosphere absorption (unit optical depth, km)[b]	Terrestrial atmosphere absorption (thermal region)[b]
X_{hf}	X-rays	X-rays	0.1–0.8	Hot corona	Flare	70–90	Mesosphere
X_{b10}	X-rays	X-rays	0.1–0.8	Corona	Active region background	70–90	Mesosphere
$XE_{10.7}$	X-rays and UV	XUV + EUV	1–40	Chromosphere, corona	Active region, plage	90–200	Lower, mid thermosphere
$E_{10.7}$	X-rays and UV	XUV + EUV	1–105	Chromosphere, corona	Active region, plage, network	90–500	Thermosphere
$*F_{10.7}$	Radio	Radio	10.7E7	Transition region, cool corona	Active region	90–500	Thermosphere
$*S_{10.7}$	UV	EUV	26–34	Chromosphere, corona	Active region, plage, network	200–300	Thermosphere
$XL_{10.7}$	X-rays and UV	X-rays + H Lyman-α	0.1–0.8, 121	Chromosphere, transition region, corona	Active region, plage, network	70–90	Mesosphere
H Lyα	UV	H Lyman-α	121	Transition region, chromosphere	Active region, plage, network	70–90	Mesosphere
E_{SRC0}	UV	FUV	125–175	Photosphere, chromosphere	Plage and network	90–125	Mesosphere, lower thermosphere
E_{SRC1}	UV	FUV	151–152	Chromosphere	Plage and network	125	Lower thermosphere
E_{SRC2}	UV	FUV	144–145	Chromosphere	Plage and network	125	Lower thermosphere
E_{SRC3} (E_{SRC})	UV	FUV	145–165	Photosphere, chromosphere	Plage and network	125	Lower thermosphere
$*M_{10.7}$	UV	MUV	280	Chromosphere	Active region	20	Stratosphere
E_{SRB}	UV	FUV + MUV	175–205	Photosphere	Plage and network	50–70	Mesosphere
E_{HRT}	UV	MUV	245–254	Photosphere	Network, background	25	Stratosphere

*Index or proxy is used in the JB2006 model exospheric temperature equation.
[a]Vernazza et al. (1976, 1981).
[b]Banks and Kockarts (1973).

and validate it against the data used to derive it. The index or proxy was then used as an input into the JB2006 atmospheric density model prototype with a least-squares best-fit time lag and within a multiple linear regression formulation as described in Bowman and Tobiska (2006) and Bowman et al. (2007). The resulting densities were compared with 18 known satellites'-derived density data over the same common time frame. After analyzing the residual error between the modeled and satellite-derived densities, and considering other factors such as operational availability of the index or proxy, only the $F_{10.7}$, $S_{10.7}$, and $M_{10.7}$ indices, along with their 81-day centered smoothed values, were selected for use in JB2006. We studied many different smoothing schemes, both centered and backward, over a multiplicity of time frames (27, 54, 90, 162 days) but found that the 81-day centered smoothing with the moving boxcar method produced the lowest residuals in our modeled-versus-derived densities. We do not yet understand the physical reason why 81-day smoothing works best, but we suggest it may represent an average time scale for solar active region evolution, which temporally varies differently than daily irradiances dominated by the 27-day solar rotation. Since JB2006 was developed as a research-grade model, the 81-day smoothing uses actual data up to 40 days prior to the current epoch. If one were to use JB2006 for times more recent than that, it is necessary to first create a forecast of daily indices that can be used in the smoothing routine. As the use-date approaches the current epoch, more

Table 2
Characteristics of daily reported solar indices

Index or proxy	Observing facility	Instrument	Observation time frame	Measurement cadence	Measurement latency	Operational availability
$*F_{10.7}$	Penticton ground observatory	Radio telescope	1947–2006	3 times/day	Up to 24 h	Yes
$*S_{10.7}$	SOHO	SEM	1996–2006	15 s	Up to 24 h	(a)
$XL_{10.7}$	GOES-12, UARS, SORCE, TIMED	XRS, SOLSTICE (2), SEE	1991–2006	1 min, 16 times/day	Up to 10 min, up to 48 h	(b)
E_{SRC}	UARS, SORCE	SOLSTICE (2)	1991–2006	16 times/day	Up to 48 h	(c)
$*M_{10.7}$	NOAA-16,17	SBUV	1991–2006	2 times/day	Up to 24 h	Yes
E_{HRT}	UARS, SORCE	SOLSTICE (2)	1991–2006	16 times/day	Up to 48 h	(c)

*Index or proxy is used in the JB2006 model exospheric temperature equation.
(a) SOHO/SEM is a NASA research instrument but provides daily irradiances on an operational cadence; GOES 13 EUVS B channel makes measurements in the same bandpass as SOHO SEM.
(b) GOES XRS is a NOAA operational instrument, whereas TIMED/SEE and SORCE/SOLSTICE are NASA research instruments providing daily irradiances on an operational measurement cadence.
(c) UARS/SOLSTICE stopped in 2005; SORCE/SOLSTICE intends to provide data for several years.

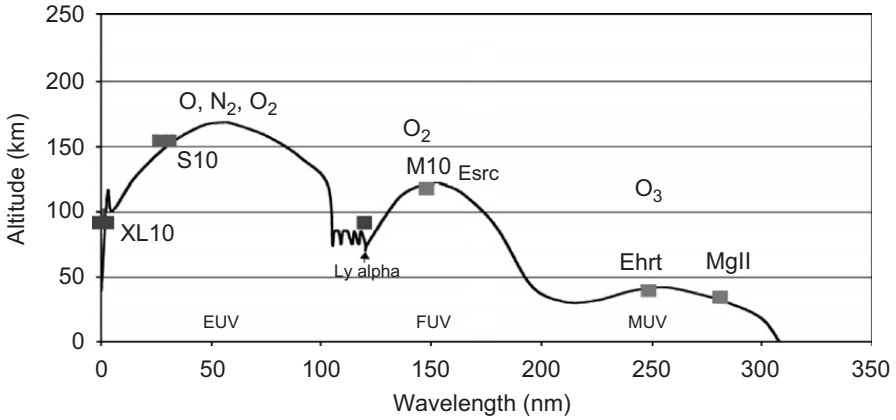

Fig. 2. Unit optical depth (altitude of maximum heating) for solar irradiances ranging from X-ray to MUV wavelengths. Neutral species that participate in heating are labeled in black, and index designators for selected bandpasses are shown in gray.

information is ingested into the smoothing from the forecast period until the current epoch is reached, at which point half of the 81-day information content is from forecast data. The uncertainty in the 81-day index grows accordingly. We describe our results for each of the solar indices that drive the JB2006 research-grade model and for indices that were additionally studied. An asterisk (*) preceding the proxy or index indicates that it is used in JB2006.

2.1. $*F_{10.7}$

The 10.7-cm solar radio flux, $F_{10.7}$, was first observed by Covington (1948) on a daily basis beginning on February 14, 1947 and is now produced daily by the Canadian National Research Council's Herzberg Institute of Astrophysics at its ground-based Dominion Radio Astrophysical Observatory located in Penticton, British Columbia. Observations of the $F_{10.7}$ flux density values are made at 18, 20 and 22 UT each day and made available through the DRAO website (contact: solar@DD2.drao.nrc.ca). The 20 UT observed (not 1 AU) values are archived at the World Data Center and were used in this study. The physical units of $F_{10.7}$ are $\times 10^{-22}\,\mathrm{W\,m^{-2}\,Hz^{-1}}$ and we use the numerical value without the multiplier as is customarily done and expressed as solar flux units (sfu). In other words, a 10.7-cm radio emission of $150 \times 10^{-22}\,\mathrm{W\,m^{-2}\,Hz^{-1}}$ is simply referred to as $F_{10.7} = 150$ sfu.

$F_{10.7}$ is the traditional solar energy proxy that has been used since Jacchia developed empirical exospheric temperature equations for atmospheric

density models, e.g., CIRA72. Its formation is physically dominated by non-thermal processes in the solar transition region and cool corona and, while it is a non-effective solar emission relative to the Earth's atmosphere, it is a useful proxy for the broad combination of chromospheric, transition region, and coronal solar EUV emissions modulated by bright solar active regions whose energies, at Earth, are deposited in the thermosphere. We use the observed archival daily values with a 1-day lag as described in Bowman and Tobiska (2006) and Bowman et al. (2007). The 1-day lag had the best correlation with satellite density residuals. All indices have been correlated to $F_{10.7}$. This is because it has become the recognized proxy for EUV and, by reporting other indices in units of $F_{10.7}$, it becomes very easy to qualitatively discern similarities and differences between proxies and indices. It is desirable to have solar indices and proxies that vary differently in time since one wants to capture the greatest range of energies from solar temperature regions.

We have created a running 81-day centered smoothed set of values using the moving boxcar method and these data are referred to as either F_{81} or F_{BAR}. In our analysis, we have used linear regression with daily $F_{10.7}$ to scale and report all other solar indices in units of sfu. Days for missing data values are not included in the regressions.

2.2. *$S_{10.7}$

The NASA/ESA Solar and Heliospheric Observatory (SOHO) research satellite operates in a halo orbit at the Lagrange Point 1 (L1) on the Earth–Sun line, approximately 1.5 million km from the Earth, and has an uninterrupted view of the Sun. One of the instruments on SOHO is the Solar Extreme-ultraviolet Monitor (SEM) that was built and is operated by University of Southern California's (USC) Space Science Center (SSC). SOHO was launched on December 2, 1995 and SEM has been making observations since December 16, 1995. As part of its continuous solar observations, the SEM instrument measures the 26–34 nm solar EUV emission with 15-s time resolution in its first-order broadband wavelength range. The orbit and solar data are both retrieved daily by USC SSC for processing in order to create daily solar irradiances with a latency of up to 24 h (Judge et al., 2001).

We have used the integrated 26–34 nm emission ($\mathrm{SOHO\_SEM_{26–34}}$) and normalized it by dividing the daily value by the common time frame mean value. The $\mathrm{SOHO\_SEM_{26–34\text{-}mean}}$ mean value for the common time frame and adjusted to 1 AU is 1.9955×10^{10} photons $\mathrm{cm^{-2}\,s^{-1}}$. The normalized value is converted to sfu through linear regression with $F_{10.7}$ and the resulting index is called $S_{10.7}$. After the end of the common time frame (June 12, 2005), a slight long-term trend is removed from the $S_{10.7}$ index to ensure similar values at the minima of solar cycles 22 and 23. $S_{10.7}$ is sometimes referred to as S_{EUV} in early conference presentations. Eq. (1) is the formulation used to derive the SOHO EUV, $S_{10.7}$. Fig. 3 shows the $S_{10.7}$ index and the S_{81} (81-day centered smoothed) values for January 1996–September 2007.

The broadband (wavelength integrated) SEM 26–34 nm irradiances, represented by the $S_{10.7}$ index, are EUV line emissions dominated by the chromospheric He II line at 30.4 nm and the coronal Fe XV line at 28.4 nm along with contributions from other chromospheric, transition region, and coronal lines. This energy principally comes from solar active regions, plage, and network. Once the photons reach the Earth, they are deposited (absorbed) in the terrestrial thermosphere mostly by atomic oxygen above 200 km. We use the daily index with a 1-day lag (the best correlation with satellite density residuals) as described in Bowman and Tobiska (2006) and Bowman et al. (2007). We suggest the 1-day lag is consistent with O diffusion timescales in the thermosphere above 180 km:

$$S_{10.7} = (-12.01) + (141.23) \times (\mathrm{SOHO\_SEM_{26-34}}/\mathrm{SOHO\_SEM_{26-34\text{-}mean}}). \quad (1)$$

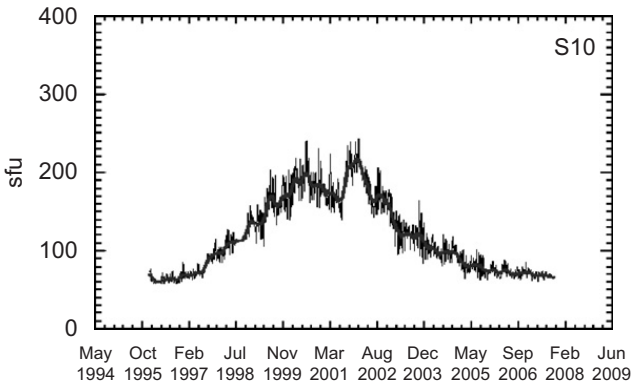

Fig. 3. $S_{10.7}$ shown in black from January 1996 to September 2007 in sfu and 81-day centered smooth shown in black bold.

2.3. E_{SRC}

The solar FUV SRC contains emission between 125 and 175 nm from the photosphere and lower chromosphere. This solar energy is deposited in the terrestrial mesosphere and lower thermosphere (80–125 km) primarily through the energy released from the dissociation of molecular oxygen.

The SRC has been observed with the SOLSTICE instruments on UARS by Rottman and Woods (1994) and on SORCE (McClintock et al., 2000). These are NASA research satellites as is the TIMED satellite that hosts the SEE instrument (Woods et al., 1994); all three are conducting long-term investigations of solar spectral irradiances. We selected a small number of irradiance ranges to study that were representative of strong lines in the SRC (144–145 and 151–152 nm) and mixed broadband emission (145–165 nm). In addition, we used wavelength binning that was consistent with SOLSTICE instrument resolution and that had the potential of being produced operationally in the future. After a comparison of 3 bands in the SRC (144–145, 151–152, 145–165 nm), we selected the 145–165 nm band (E_{SRC3} in Table 1, also sometimes called E_{SRC}) as a representative wavelength range for the remainder of the SRC. The emission in this band is mostly deposited in the 100–125 km altitude region.

For our analysis, we integrated the daily SOLSTICE 145–165 nm emission from UARS and SORCE, created a normalized index by dividing the daily value by the common time frame mean value, $\mathrm{SOLSTICE}_{145\text{–}165\text{-mean}}$, which has a value of 2.1105×10^{11} photons $\mathrm{cm}^{-2}\,\mathrm{s}^{-1}$. Next, we performed a linear regression with $F_{10.7}$ to report the index in sfu. E_{SRC}, as shown in Eq. (2), is the result and we used this index with a 5-day lag, which gave the best empirical fit between the index and the satellite drag density residuals (Bowman et al., 2007). The physical reason for this 5-day lag is still unclear, but we suggest it may be related to the timescale of atomic oxygen diffusion after it has been formed from the SRC dissociation of O_2. Fig. 4 shows the E_{SRC} and the E_{SRC81} (81-day centered smoothed) values as the combination of UARS, TIMED, and SORCE data. In developing Eq. (2), we used only UARS and SORCE SOLSTICE data since it had lower uncertainty compared with TIMED SEE data in the 145–165 nm FUV wavelength range:

$$E_{\mathrm{SRC}} = (-784.03) + (909.34) \times (\mathrm{SOLSTICE}_{145-165}/\mathrm{SOLSTICE}_{145-165\text{-mean}}). \quad (2)$$

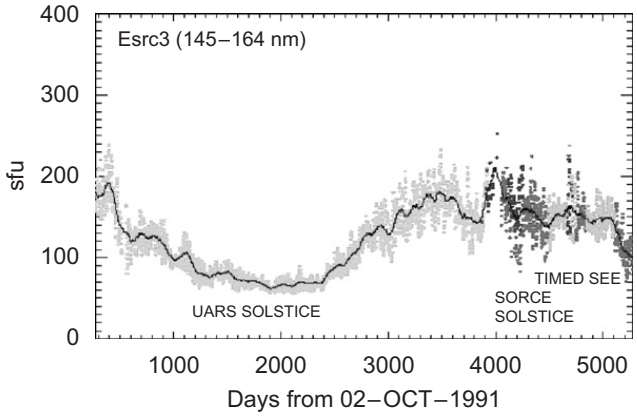

Fig. 4. E_{SRC} shown from 1991 into 2005 in sfu and 81-day centered smooth shown in black.

2.4. E_{HRT}

The solar middle ultraviolet (MUV) Hartley Band (HB) contains emission between 245 and 254 nm from the photosphere. This solar energy is deposited in the terrestrial stratosphere (30–40 km) primarily through the energy released from the dissociation of ozone. The solar HB emissions have been observed daily by the SOLSTICE instrument on the UARS and SORCE satellites.

For our analysis, we have integrated the daily SOLSTICE 245–254 nm emission and created a normalized index by dividing the daily value by the common time frame mean value, $\mathrm{SOLSTICE}_{245\text{–}254\text{-mean}}$, which has a value of 3.1496×10^{13} photons $\mathrm{cm}^{-2}\,\mathrm{s}^{-1}$. Next, we performed a linear regression with $F_{10.7}$ to report the index in sfu. E_{HRT}, as shown in Eq. (3), is the result and we have used this index with multiple-day lags but with no apparent effect upon reducing the JB2006-modeled residuals with respect to the satellite-derived density data:

$$E_{\mathrm{HRT}} = (-726.27) + (851.57)\mathrm{HB}_{245-254}/\mathrm{HB}_{245-254\text{-mean}}. \quad (3)$$

2.5. $*M_{10.7}$

The NOAA series operational satellites, e.g., NOAA 16 and NOAA 17, host the solar backscatter ultraviolet (SBUV) spectrometer that has the objective of monitoring ozone in the Earth's lower atmosphere. In its discrete operating mode, a diffuser screen is placed in front of the instrument's aperture in order to scatter solar MUV radiation near 280 nm into the instrument.

This solar spectral region contains both photospheric continuum and chromospheric line

emissions. The chromospheric Mg II *h* and *k* lines at 279.56 and 280.27 nm, respectively, and the weakly varying photospheric wings or continuum longward and shortward of the core line emission, are operationally observed by the instrument. On the ground, the Mg II core-to-wing ratio (cwr) is calculated between the variable lines and nearly non-varying wings. The result is a measure of chromospheric and some photospheric solar active region activity that is theoretically independent of instrument sensitivity change through time, is referred to as the Mg II cwr, and is provided daily by the NOAA Space Weather Prediction Center (SWPC—formerly Space Environment Center, SEC) (Viereck et al., 2001).

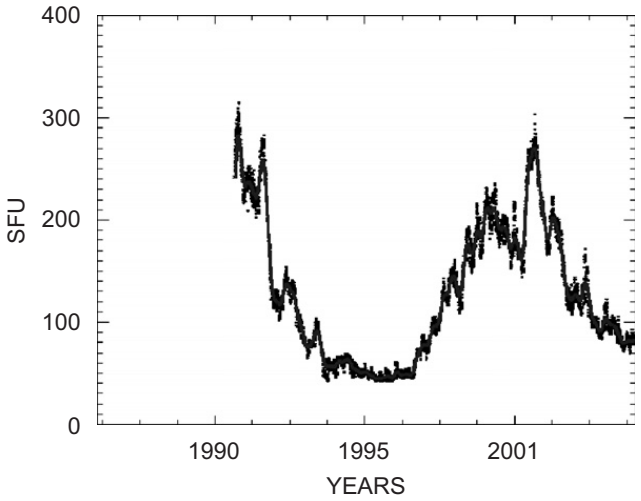

Fig. 5. $XL_{10.7}$ shown from 1991 into 2005 in sfu in black and the 81-day centered smooth shown in dark gray.

The ratio is an especially good proxy for some solar FUV and EUV emissions. Our analysis has found that it can represent very well the photospheric and lower chromospheric solar FUV SRC emission (Bowman et al., 2007). We have taken the Mg II cwr and performed a linear regression with $F_{10.7}$ for the common time frame to derive the $M_{10.7}$ index that is the Mg II cwr reported in $F_{10.7}$ units. Eq. (4) provides the calculation of $M_{10.7}$ based on the NOAA 16 SBUV Mg II cwr data. In deriving the $M_{10.7}$ index, we remove a slight long-term trend

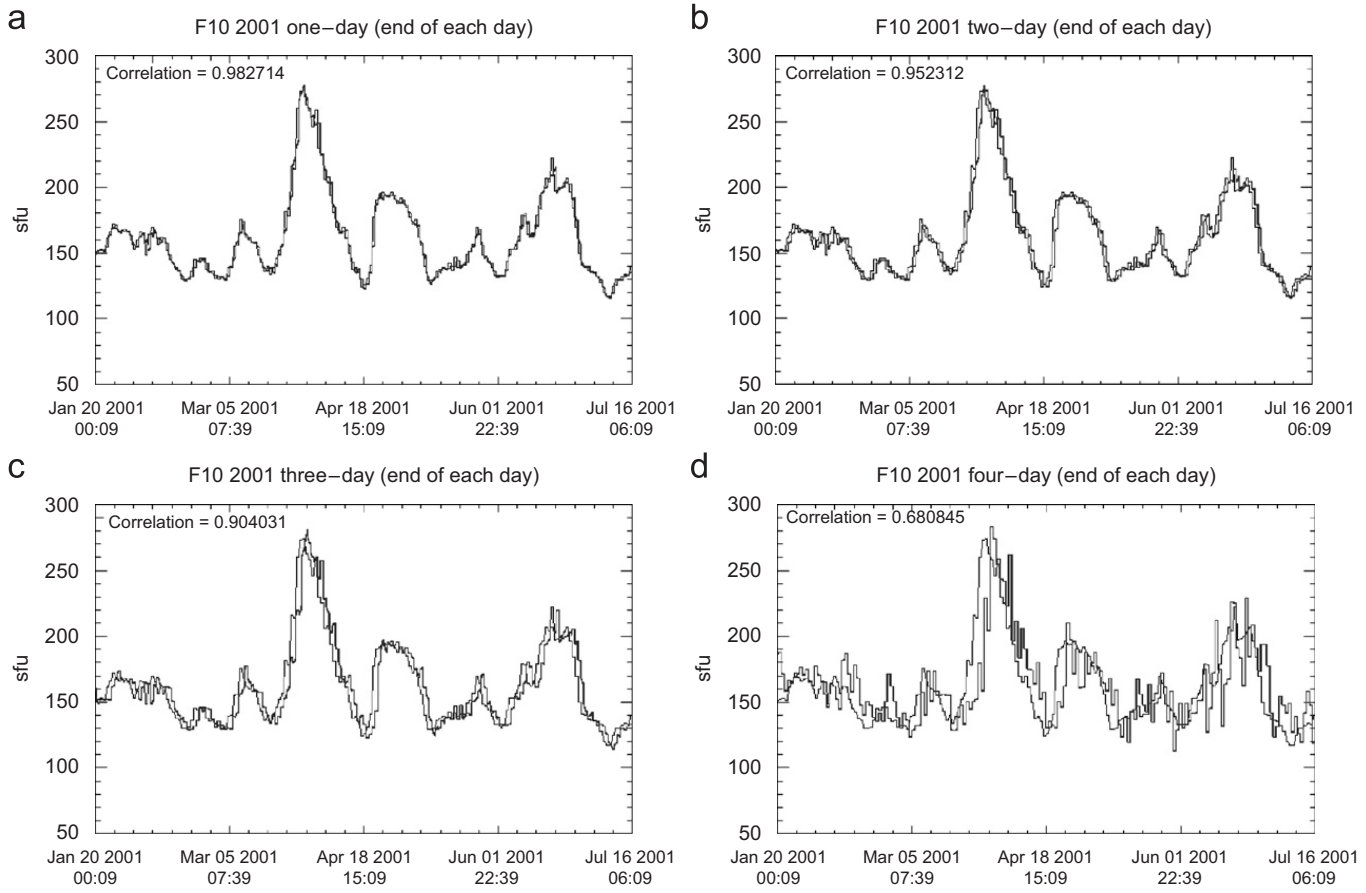

Fig. 6. Predicted (dark gray) and actual (black) $F_{10.7}$, with correlation coefficients [*R*], for January 20–July 15, 2001 at (a) 24 h [0.98], (b) 48 h [0.95], (c) 72 h [0.90] and (d) 96 h [0.68].

to ensure similar values at the minima of solar cycles 22 and 23. The trend differences are negligible in 1996–1997 and are on the order of 10% by 2007. The source of the trend is still unknown, but we suggest it may be related to the diffuser screen illumination geometry on NOAA 16 that may have changed with time. We use this daily $M_{10.7}$ index with a 5-day lag as described in Bowman and Tobiska (2006) and Bowman et al. (2007) as a proxy for E_{SRC} since the latter is not operationally available:

$$M_{10.7} = (-1943.85) + (7606.56)\mathrm{Mg\_II}_{\mathrm{NOAA16}}. \quad (4)$$

2.6. $XL_{10.7}$

The X-ray spectrometer (XRS) instrument is part of the instrument package on the GOES series operational spacecraft. The XRS on GOES spacecraft provide the historical through current epoch 0.1–0.8 nm solar X-ray emission with 1-min cadence and 5-min latency. These data, used for flare detection, are continuously reported by NOAA SWPC at the website http://www.swpc.noaa.gov/.

X-rays in the 0.1–0.8 nm range come from the cool and hot corona and are typically a combination of both a very bright solar active region background that varies slowly (days to months) plus flares that vary rapidly (minutes to hours), respectively. The photons arriving at the Earth are primarily absorbed in the mesosphere and lower thermosphere (80–90 km) by molecular oxygen and nitrogen, where they ionize those neutral constituents to create the ionospheric D-region.

Tobiska and Bouwer (2005) developed an index of the solar X-ray active region background, without the flare component, for operational use. This is called the X_{b10} index and is used to represent the daily energy that is deposited into the mesosphere and lower thermosphere.

The 0.1–0.8 nm X-rays are a major energy source in these atmospheric regions during high solar activity but relinquish their dominance to the competing hydrogen (H) Lyα emission during moderate and low solar activity. Lyα is also deposited in the same terrestrial atmospheric layers, is created in the solar upper chromosphere and

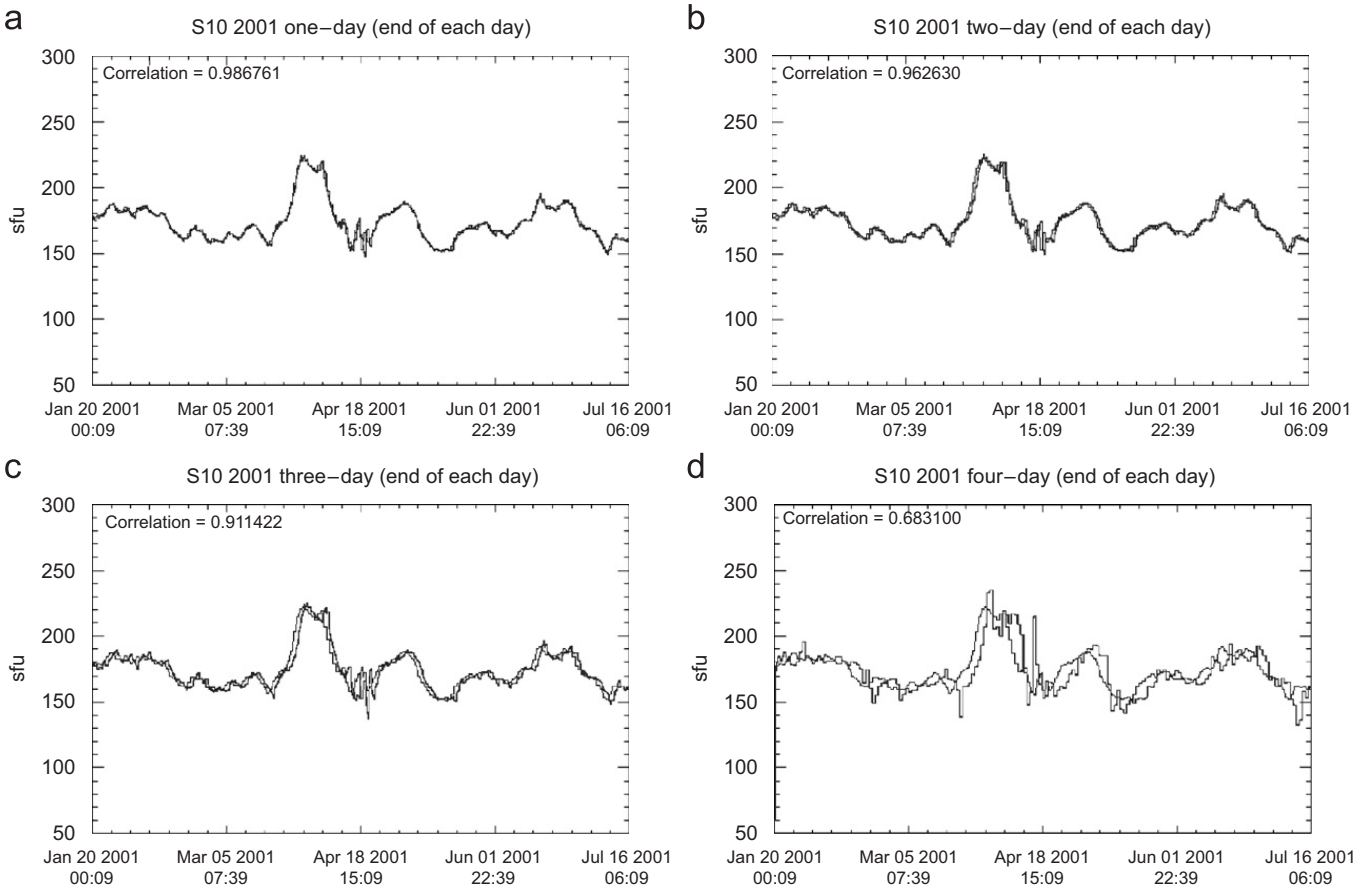

Fig. 7. Predicted (dark gray) and actual (black) $S_{10.7}$, with correlation coefficients [R], for January 20–July 15, 2001 at (a) 24 h [0.99], (b) 48 h [0.96], (c) 72 h [0.91] and (d) 96 h [0.68].

transition region, and demarcates the EUV from the FUV spectral regions. It is formed primarily in solar active regions, plage, and network; the photons, arriving at Earth, are absorbed in the mesosphere and lower thermosphere, where they dissociate nitric oxide (NO) and participate in water (H_2O) chemistry. Lyα has been observed by the SOLSTICE instrument on the UARS and SORCE satellites, as well as by the SEE instrument on TIMED (Woods et al., 2000).

Since these two solar emissions are competing drivers to the mesosphere and lower thermosphere, we have developed a mixed solar index of the X_{b10} and Lyα. It is weighted to reflect mostly X_{b10} during solar maximum and to reflect mostly Lyα during moderate and low solar activity. The independent, normalized F_{81} (81-day centered smoothed $F_{10.7}$ divided by the common time frame mean value, i.e., $F_{81\text{–normalized}}$) is used as the weighting function and multiplied with the X_{b10} and Lyα as fractions to their solar maximum values. Eq. (5) provides the $XL_{10.7}$ index reported in sfu. Over the common time frame, we tested this daily index with multi-day lags and the 8-day lag was found to have the strongest signal in the satellite drag density residuals after all other known signals were removed. It improved by a few percent of the JB2006-modeled residuals versus the derived satellite densities. However, due to the operational complexity of producing this index, we decided not to include it in the final formulation of JB2006. Fig. 5 shows the $XL_{10.7}$ and the XL_{81} values from 1991 into 2005:

$$XL_{10.7} = \{F_{81-\text{normalized}}(X_{b10}/X_{b10-\max}) + (1 - F_{81-\text{normalized}})(\text{Ly}\alpha/\text{Ly}\alpha_{\max})\}F_{81}. \quad (5)$$

3. Forecasting solar indices and proxies

As noted above, the $F_{10.7}$, $S_{10.7}$, and $M_{10.7}$ proxies and indices, along with their 81-day centered smoothed values, are used as the solar inputs for

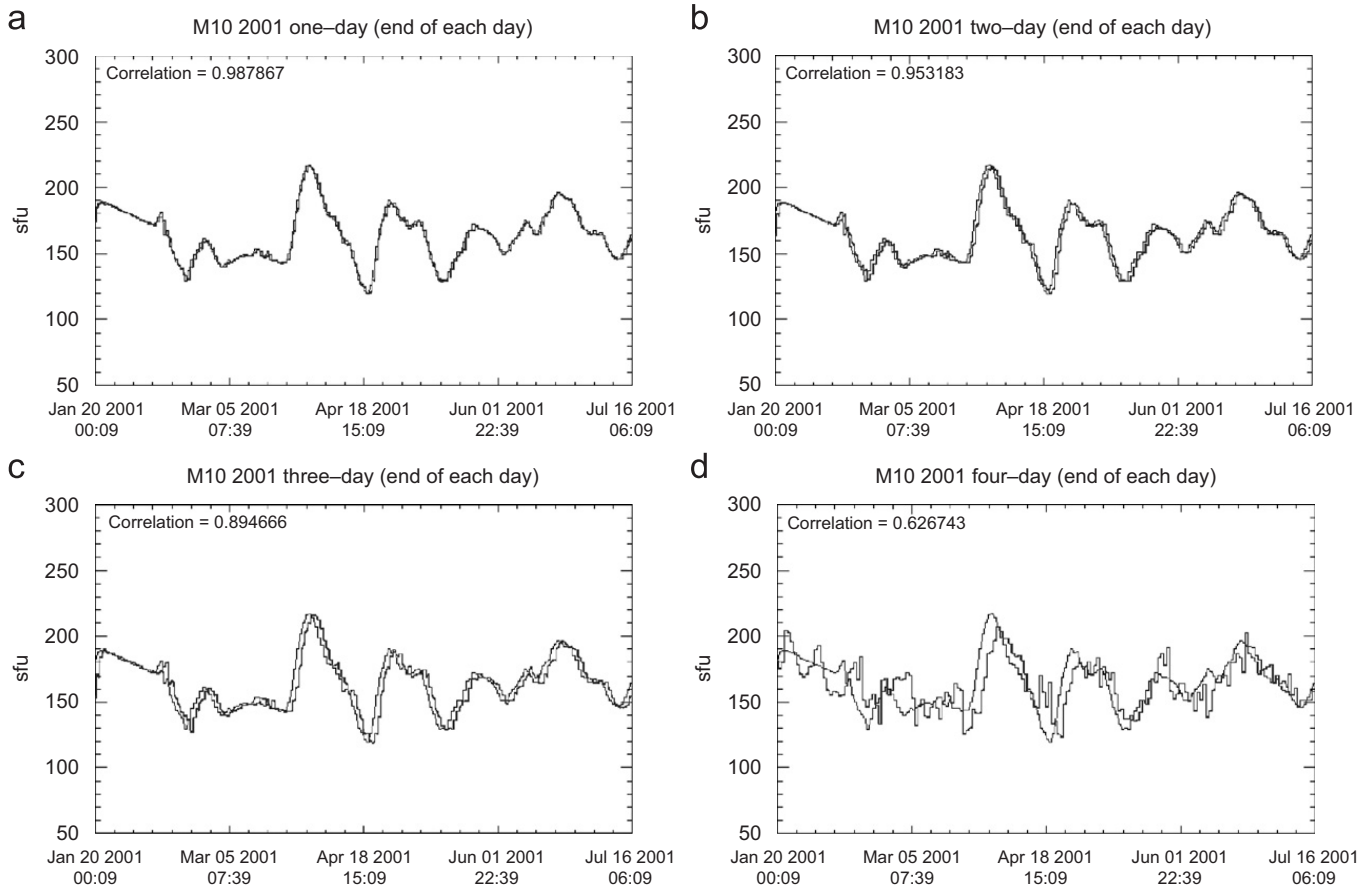

Fig. 8. Predicted (dark gray) and actual (black) $M_{10.7}$, with correlation coefficients [R], for January 20–July 15, 2001 at (a) 24 h [0.99], (b) 48 h [0.95], (c) 72 h [0.89], and (d) 96 h [0.63].

the JB2006 empirical thermospheric density model. An additional motivation has been to provide real-time and forecast solar indices, along with historical values, for thermospheric density and ionospheric applications. Space Environment Technologies (SET) has developed forecast algorithms to provide these three indices through the hybrid (empirical, physics-based, and data assimilative) Solar Irradiance Platform (SIP), which incorporates what was formerly the SOLAR2000 (S2K) (Tobiska et al., 2000; Tobiska, 2004; Tobiska and Bouwer, 2006) and other models. We report on those forecast algorithms and their success here.

SET has developed seven operational forecasting principles that are used in the production of the $F_{10.7}$, $S_{10.7}$, and $M_{10.7}$ solar indices and proxies:

(1) time domain definitions of past, present, and future are demarcated with identifiable granularity, cadences, and latencies relative to the current epoch;
(2) information redundancy is obtained using multiple data streams;
(3) data reliability is guaranteed only when quality forecasts flow uninterruptedly despite subsystem anomalies;
(4) system robustness is achieved only when an operational forecasting system is modular, manageable, and extensible using tiered architecture;
(5) technology readiness levels (TRLs) define the evolution of models and data to move from research grade to standalone operational maturity;
(6) geophysical validation is achieved when an output forecast represents the geophysical conditions within specified limits; and
(7) operational verification is achieved when an output forecast meets the user-specified requirements' intent.

The foundation for the empirical forecasting in SET's Forecast Generation 2 Delivery 3.9 (FGen2/D3.9) is persistence and recurrence, and this is achieved using linear prediction for $F_{10.7}$, $S_{10.7}$, and $M_{10.7}$. We developed and tested a combination of

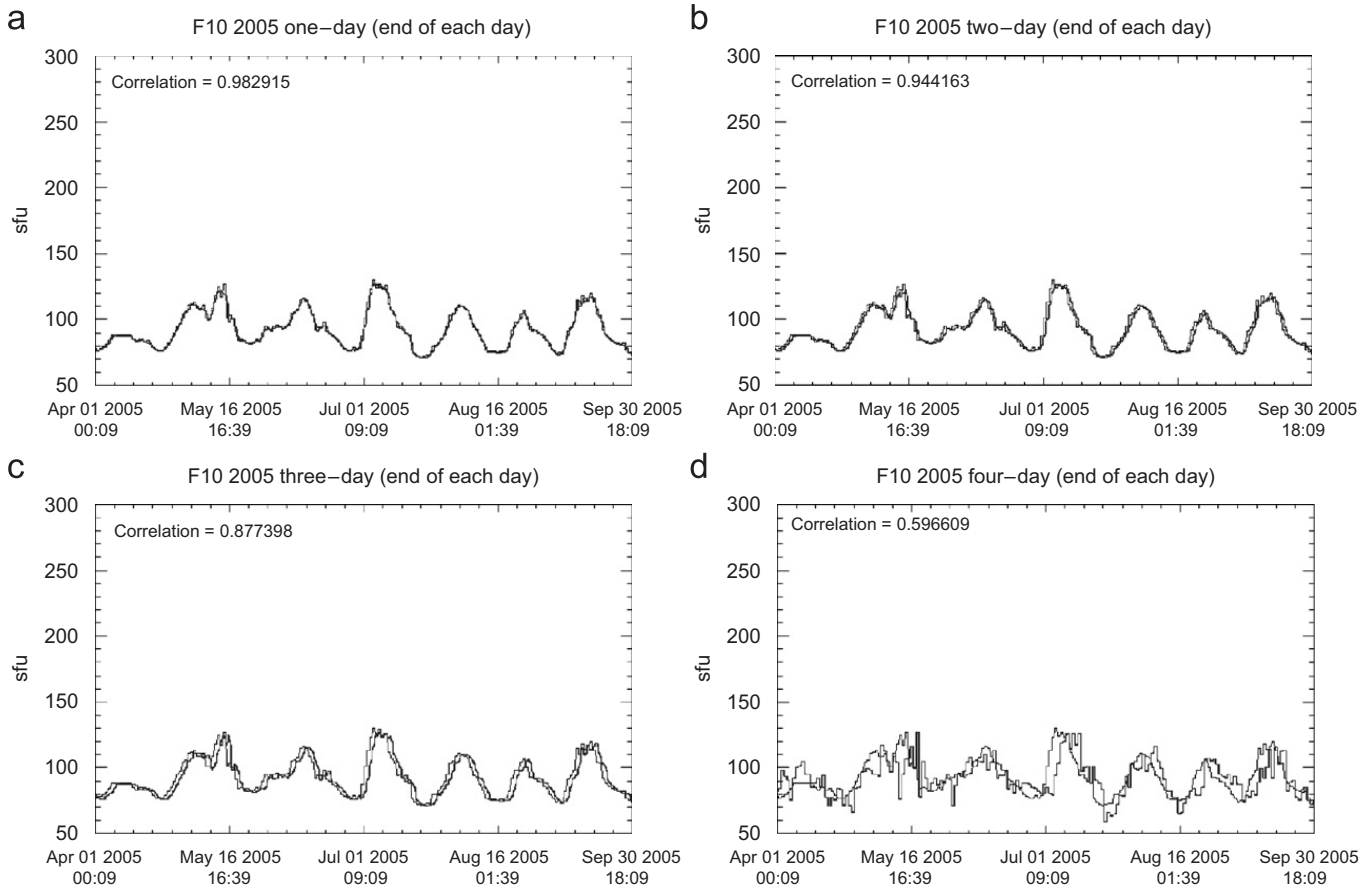

Fig. 9. Predicted (dark gray) and actual (black) $F_{10.7}$, with correlation coefficients [R], for April 1–September 30, 2005 at (a) 24 h [0.98], (b) 48 h [0.94], (c) 72 h [0.88] and (d) 96 h [0.60].

algorithms based on SOHO/EIT 30.4 nm image analysis, including limb and center of disk data for active regions, plage, network, and background, as well as singular value decomposition routines coupled with empirical long-term active region evolution functions. This technique holds promise for improving intermediate-term forecasts longer than 3 days. However, in the 0–72 h time frame, the Eq. (6) generic formulation of a linear predictive technique proved to be the most successful method for predicting non-flare irradiance conditions for $F_{10.7}$, $S_{10.7}$, and $M_{10.7}$. Tobiska and Bouwer (2005) separately describe flare evolution predictions. We note that

$$x_t = \varphi_1 x_{t-1} + \varphi_2 x_{t-2} + \cdots + \varphi_P x_{t-P} + w_t, \quad (6)$$

where x is the solar index value at a forecast time t, P is the most recent value to be used, φ are linear coefficients, and w is a residual error term. Out to 48 h prediction we used the three most recent days of index values. Between 48 and 96 h we used the last five solar rotations (137 days) as the most recent values. Our predictive results for high solar activity between January 20 and July 15, 2001 are shown in Figs. 6–8 for the $F_{10.7}$, $S_{10.7}$, and $M_{10.7}$ indices and proxies, respectively. Our results for low solar activity between April 1 and October 1, 2005 are shown in Figs. 9–11 for the $F_{10.7}$, $S_{10.7}$, and $M_{10.7}$ indices and proxies, respectively. Table 3 summarizes the regression coefficients from our forecasts for both high (2001) and low (2005) solar activity. The forecasts were generated every 6 h throughout the 6-month duration of each solar activity period. There is a 3-h time granularity in each forecast epoch. We note that the low solar activity period (2005) also has marked 27-day variation, though at a lower absolute flux level. The linearity of the forecast technique, using the assumption of persistence, provides reduced uncertainty when the magnitude of 27-day variability is small.

We note that the nowcast correlation coefficients are not identically 1.0000 in Table 3. This is because a nowcast at the current, 0 h, epoch is actually a forecast. Operational data come in asynchronously

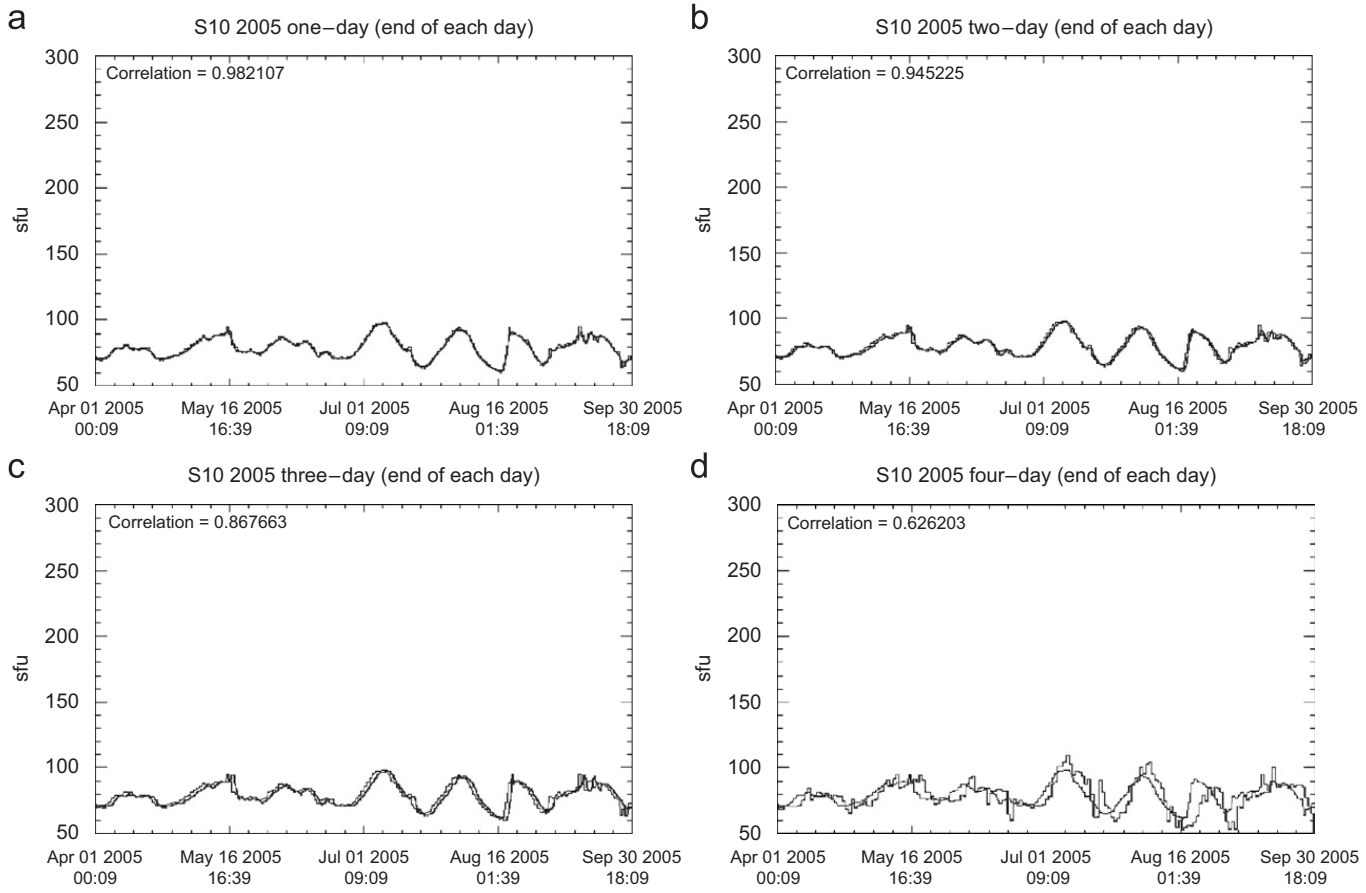

Fig. 10. Predicted (dark gray) and actual (black) $S_{10.7}$, with correlation coefficients [R], for April 1–September 30, 2005 at (a) 24 h [0.98], (b) 48 h [0.95], (c) 72 h [0.87] and (d) 96 h [0.63].

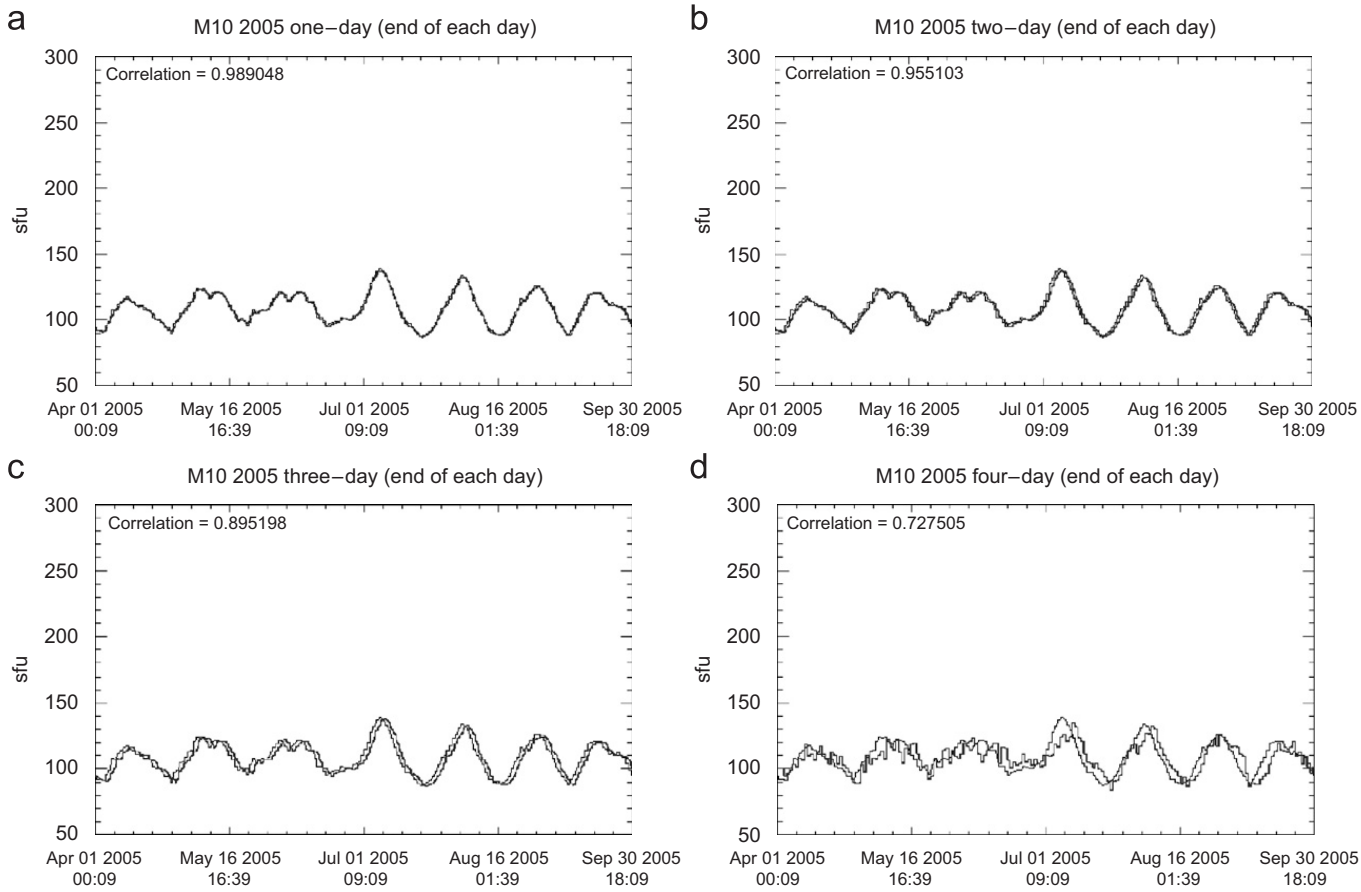

Fig. 11. Predicted (dark gray) and actual (black) $M_{10.7}$, with correlation coefficients [R], for April 1–September 30, 2005 at (a) 24 h [0.99], (b) 48 h [0.96], (c) 72 h [0.90] and (d) 96 h [0.73].

Table 3
Correlation coefficients (R) of forecast solar indices and proxies

Index or proxy	2001 nowcast	2001 24-h	2001 48-h	2001 72-h	2001 96-h	2005 nowcast	2005 24-h	2005 48-h	2005 72-h	2005 96-h
$F_{10.7}$	0.99	0.98	0.95	0.90	0.68	0.98	0.98	0.94	0.88	0.60
$S_{10.7}$	0.99	0.99	0.96	0.91	0.68	0.98	0.98	0.95	0.87	0.63
$M_{10.7}$	0.99	0.99	0.95	0.89	0.63	0.99	0.99	0.96	0.90	0.73

during the preceding nowcast time interval defined by SET as −24 h up to the current epoch, 0 h. Since operational solar indices are derived from multiple data sets, there is often a time lag between the most recent values driving the forecast and the current epoch. In some cases, there may be a 24-h lag between the current epoch nowcast and the most recent data used to create it. As a result, the correlation coefficients at the nowcast epoch are not 1.00000. The FGen2 algorithms make a prediction of solar indices and proxies at 3-h intervals into the future out to 96 h. We show "snapshots" of the correlation coefficients at 24, 48, 72, and 96 h in Table 3.

There has been substantial improvement in near-term forecasting over the past 5 years as evidenced in Figs. 6–11 and Table 3, where most of the correlation coefficients are well above 0.90. To demonstrate the improvement through time, a comparison is useful between the 3-day forecasts of $F_{10.7}$ during the January 20 to July 15, 2001 high solar activity test period. Three forecast results are shown: (1) NOAA SWPC/Air Force Weather Agency (AFWA) results that were state-of-the-art

in 2001, (2) SET's (HASDM) fully operational (TRL 9) FGen1X forecasts in 2003, and (3) SET's FGen2 prototype operational (TRL 8) forecasts (2006). Fig. 12 graphically shows the improvement in the forecasts at the 24, 48, and 72-h epochs. Table 4 shows the $1-\sigma$ percent uncertainty for the NOAA SWPC/AFWA, SET FGen1X (HASDM), and SET FGen2 predictions. FGen2 clearly makes improved predictions compared with the other two.

A summary view of all three JB2006 indices and proxies from January 1996 to October 2007 is shown in Fig. 13 compared with each other. The SIP v2.32 application provides these historical and real-time $F_{10.7}$, $S_{10.7}$, and $M_{10.7}$ values and is available for download at the http://spacewx.com SIP quicklink.

4. Conclusion

This work produces historical and real-time solar irradiance proxies and indices for use in the research-grade model for thermospheric densities, JB2006. The $F_{10.7}$, $S_{10.7}$, and $M_{10.7}$ indices' and proxies' derivations as well as use are described. The $F_{10.7}$ proxy has existed for many years and, with a 1-day lag, continues to be a useful surrogate for cool corona and transition region XUV–EUV solar irradiances depositing their energy throughout the thermosphere. The new $S_{10.7}$ index of chromospheric EUV solar irradiances, with a 1-day lag, significantly improves the estimation of the solar energy that heats atomic oxygen in the terrestrial thermosphere. The new $M_{10.7}$ proxy for photosphere/lower chromosphere FUV solar irradiances, based on the Mg II cwr and used with a 5-day lag, significantly improves the estimation of the solar energy that dissociates molecular oxygen in the terrestrial lower thermosphere. $1-\sigma$ forecast uncertainties out to 72-h are 1–10% for all three proxies/indices in high as well as low solar activity conditions.

Our objective of providing an operational, system-level capability that reduces risk from space weather phenomena related to solar FUV–XUV irradiance variability and their heating through dissociation and ionization of upper atmosphere species has achieved significant success. These three indices and proxies, when used in a JB2006-type thermospheric density model, provide significantly improved 72-h thermospheric density forecasts for operational satellite users. Our Forecast Generation 2 (FGen2) coupled system of data and models is at TRL 8, i.e., a system prototype is running in a relevant operational environment, is well integrated with collateral and ancillary systems, and has limited documentation. It is designed to meet the SSA challenges of *making measurements rapidly*, *interpreting them quickly*, and *reacting to the*

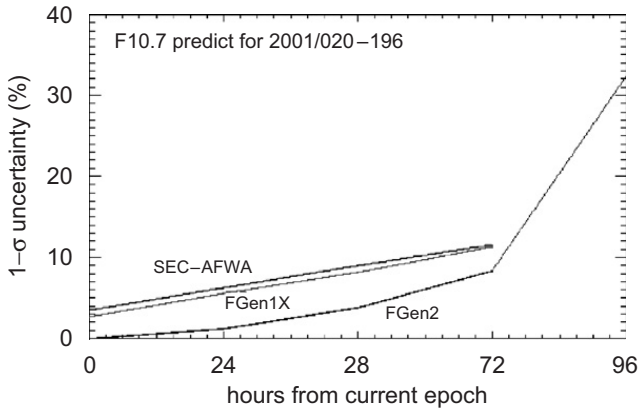

Fig. 12. $F_{10.7}$ $1-\sigma$ percentage uncertainty in predictions by NOAA SEC/AFWA (top line), SET FGen1X (light gray middle line), and SET FGen2 (lowest dark line extending to 96 h) every 3 h from January 20 to July 15, 2001.

Table 4
$1-\sigma$ percentage uncertainty at selected forecast epochs[a]

Hours from current epoch	+00	+24	+48	+72	+96
NOAA SEC/AFWA	3.6	6.3	9.0	11.7	–
FGen1X	2.7	5.6	8.2	11.4	–
FGen2	0.0	1.3	3.9	8.4	32.5

[a]For high solar activity January 20 to July 15 2001.

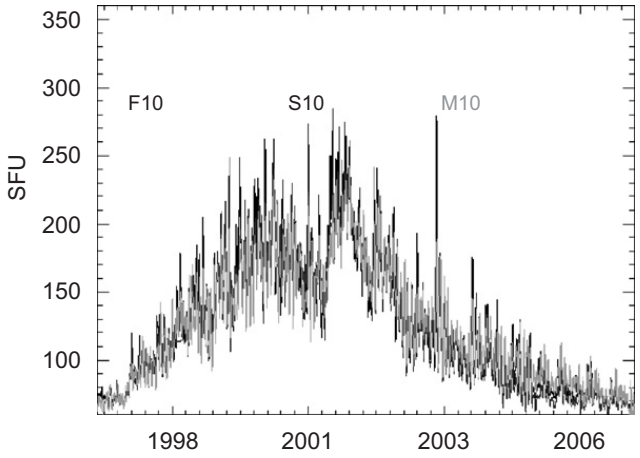

Fig. 13. The $F_{10.7}$ (black), $S_{10.7}$ (medium gray), and $M_{10.7}$ (light gray) from January 1996 to October 2007 are compared with each other.

real-time and predicted information with appropriate and timely actions.

Acknowledgments

Support for this work has been provided by the Contract GS-23F-0195N order delivery FA2550-06-F-8001 and Contract FA2550-07-C-8006. The leadership provided by the US Air Force Space Battlelab with its Sapphire Dragon Initiative has provided the organizational foundation for the breakthroughs in this work. We thank Tom Woods and the UCB/LASP instrument teams for graciously providing UARS/SOLSTICE, TIMED/SEE, SORCE/SOLSTICE data. We thank Darrell Judge, Andrew Jones, and Leonid Didkovsky of the USC/SSC SOHO/SEM team for graciously providing SEM data. The historical indices described here for input to the JB2006 model, as well as the model Fortran source code, are provided by SET at the JB2006 link on the website http://spacewx.com. The Solar Irradiance Platform (SIP) provides historical, real-time, and forecast daily JB2006 indices and proxies, as well as full spectral irradiances and real-time solar monitoring for satellite and communication system operations. It can be downloaded at the http://spacewx.com SIP quick link.

References

Banks, P., Kockarts, G., 1973. Aeronomy. Academic Press, New York.

Barth, C.A., Tobiska, W.K., Rottman, G.J., White, O.R., 1990. Comparison of 10.7 cm radio flux with SME solar Lyman alpha flux. Geophysical Research Letters 17, 571–574.

Bishop, G.J., Mazzaella, A.J., Secan, J.A., 2005. GPS TEC errors for models and operations. In: Goodman, J.M. (Ed.), 11th International Ionospheric Effects Symposium, IES2005. JMG Associates, pp. 790–797.

Bowman, B.R., Tobiska, W.K., 2006. Improvements in modeling thermospheric densities using new EUV and FUV solar indices. AAS 06-237.

Bowman, B.R., Tobiska, W.K., Marcos, F.A., 2006. A new empirical thermospheric density model JB2006 using new solar indices. AIAA 2006-6166.

Bowman, B.R., Tobiska, W.K., Marcos, F.A., Valladares, C., 2007. The JB2006 empirical thermospheric density model. Journal of Atmospheric and Solar-Terrestrial Physics, this issue, doi:10.1016/j.jastp.2007.10.002.

Center for Integrated Space Weather Modeling, 2003. First Annual Report, 8/1/2002–7/31/2003, Center for Space Physics, Boston University, Boston.

COSPAR International Reference Atmosphere 1972 (CIRA72), 1972. Compiled by the COSPAR Working Group IV. North-Holland Publishing Co., Amsterdam.

Covington, A.E., 1948. Solar noise observations on 10.7 cm. Proceedings of the I.R.E. 36, 454.

Goodman, J.M., 2005. Space Weather and Telecommunications. Springer, New York.

IS 21348:2007, 2007. Space Environment (Natural and Artificial)—Process for Determining Solar Irradiances. International Standards Organization (ISO), Geneva.

Judge, D.L., Ogawa, H.S., McMullin, D.R., Gangopadhyay, P., Pap, J.M., 2001. The SOHO CELIAS/SEM EUV database from SC23 minimum to the present. Advances in Space Research 29 (12), 1963.

McClintock, W.E., Rottman, G.J., Woods, T.N., 2000. SOLar Stellar Irradiance Comparison Experiment II (SOLSTICE II) for the NASA earth observing system's solar radiation and climate experiment mission. SPIE Proceedings 4135, 225.

Pardini, C., Tobiska, K., Anselmo, L., 2006. Analysis of the orbital decay of spherical satellites using different solar flux proxies and atmospheric density models. Advances in Space Research 37 (2), 392–400.

Rottman, G.J., Woods, T.N., 1994. The UARS SOLSTICE. SPIE Proceedings 2266, 317.

Schmidtke, G., 1976. Geophysical Research Letters 3, 573.

The National Space Weather Program, 2000. The Implementation Plan, second ed. National Space Weather Program Council, Office of the Federal Coordinator for Meteorology, FCM-P31-2000.

Tobiska, W.K., 1988. A solar extreme ultraviolet flux model. Ph.D. Thesis, Department of Aerospace Engineering, University of Colorado, 1988.

Tobiska, W.K., 2001. Validating the Solar EUV Proxy, E10.7. Journal of Geophysical Research 106 (A12), 29969–29978.

Tobiska, W.K., 2002. New developments in solar irradiance proxies for operational space weather. In: Fourth Thermospheric/Ionospheric Geospheric Research (TIGER) Symposium (Internet), June 10–14, 2002, 〈http://www.ipm.fraunhofer.de/~english/meetings/workshops/tiger/〉 or 〈http://spacewx.com〉 publications link.

Tobiska, W.K., 2003. Forecasting of space environment parameters for satellite and ground system operations. In: AIAA Aerospace Sciences Meeting, Reno, AIAA 2003-1224.

Tobiska, W.K., 2004. SOLAR2000 irradiances for climate change, aeronomy, and space system engineering. Advances in Space Research 34, 1736–1746.

Tobiska, W.K., 2005. Systems-level space environment specification for satellite and ground system operations. In: AIAA Aerospace Sciences Meeting, Reno, AIAA-2005-0069.

Tobiska, W.K., Bouwer, S.D., 2005. Solar flare evolution model for operational users. In: Goodman, J.M. (Ed.), 2005 Ionospheric Effects Symposium, JMG Associates, 76pp.

Tobiska, W.K., Bouwer, S.D., 2006. New developments in SOLAR2000 for space research and operations. Advances in Space Research 37 (2), 347–358.

Tobiska, W.K., Woods, T., Eparvier, F., Viereck, R., Floyd, L., Bouwer, D., Rottman, G., White, O.R., 2000. The SOLAR2000 empirical solar irradiance model and forecast tool. Journal of Atmospheric and Solar-Terrestrial Physics 62, 1233–1250.

Vernazza, J.E., Avrett, E.H., Loeser, R., 1976. Structure of the solar chromosphere: II. The underlying photosphere and temperature-minimum region. Astrophysical Journal Supplement Series 30, 1–60.

Vernazza, J.E., Avrett, E.H., Loeser, R., 1981. Structure of the solar chromosphere: III. Models of the EUV brightness components of the quiet Sun. Astrophysical Journal Supplement Series 45, 635–725.

Viereck, R., Puga, L., McMullin, D., Judge, D., Weber, M., Tobiska, W.K., 2001. The Mg II index: a proxy for solar EUV. Geophysical Research Letters 28 (7), 1342.

Woods, T.N., Rottman, G.J., Roble, R.G., White, O.R., Solomon, S.C., Lawrence, G.M., Lean, J., Tobiska, W.K., 1994. TIMED solar EUV experiment. SPIE Proceedings 2266, 467.

Woods, T.N., Tobiska, W.K., Rottman, G.J., Worden, J.R., 2000. Improved solar Lyman a irradiance modeling from 1947 through 1999 based on UARS observations. Journal of Geophysical Research 105, 27195.